



# Formation of multilayer structure in metallic glass nanospheres

Yiyang Zhu, Hao Wang, Linggang Wu, and Mo Li\*

## Impact statement

Metallic glasses (MGs) are considered as homogeneous and disordered without any long-range atomic packing. Here, we report the development of the onion-like, multilayered atomic structure with a one-dimensional spherical periodic order along the radial direction in MG spheres. The layering transition occurs spontaneously as driven by the surface tension at all ranges of temperatures below the glass-transition temperature. The ordering depends on the radius of the spheres, ranging from a few atomic layers in the large spheres to fully ordered in the smaller ones. The ordering phenomenon is a rare demonstration of the liquid-like behavior in the amorphous solid that blurs the boundary between the solid and liquid in nanoscales. In particular, the multilayered structure could be used in developing functional catalysts and friction or wear-resistant materials.

Atomic structure is a crucial part for the structure–property relations in fabrication and utilization of nanoscale particles. Different from the widely known one-layer core–shell model in crystalline nanoparticles, we report here a multilayer atomic structure formed in metallic glass nanoparticles. The multilayers are characterized by density modulations along the radial direction, while the underlying atomic structure still remains amorphous. As an example, the  $\text{Cu}_{64}\text{Zr}_{36}$  metallic glass nanospheres are investigated under a wide range of temperatures and sizes using molecular dynamics simulation. We found that the homogeneous amorphous structure undergoes a transition from a single surface core–shell structure to a multilayer structure with a well-defined one-dimensional periodicity when the particles are cooled through the glass transition. This unique layered atomic packing is closely correlated to the variation of the internal stress induced by the surface stress. The layered structure is also accompanied by the property modulation as well as chemical segregation on surface regions.

## Introduction

Metallic glass (MG) nanowires and nanoparticles have captured much interest recently as the decreasing feature size introduces many superior electronic, optical, catalytic, and mechanical properties over the corresponding bulk materials.<sup>1–3</sup> Some of the functionalities, such as those in catalysis and friction, are enhanced tremendously and become highly desirable owing to the structural isotropy and easy processing of the glassy material. As most applications of the nanoscale materials pivot on the ever-increasing specific surfaces, the surface atomic structure is crucial to understanding and utilizing MGs in nanoscales. Many models have been proposed to describe the atomic packing in bulk MGs in the last decades,<sup>4–7</sup> most of which focus on the short-range atomic structure in the homogeneous MG. Not much is known for the atomic structures of the surfaces and near-surface regions in nanoparticles or

wires. As known for crystalline nanomaterials, once a surface forms, the surface tension arises, and the atoms rearrange themselves as driven by the unbalanced forces originated from the surface. These forces make changes in surface composition, energy, and stresses that are different from the bulk. Many of these structural changes are observed in crystalline materials also, such as faceting, due to the obvious crystalline (re)order, and surface phase transitions.<sup>8</sup> In contrast, only a few works paid attention to surface and near-surface atomic structures in amorphous materials<sup>9,10</sup> because of the lack of interest in finding any “structural change” in already structure-less materials such as the MGs and the technical difficulties in detecting the structural change due to the absence of the Bragg diffraction in the disordered material. As more and more amorphous nanoscale materials are synthesized, and their unique

Yiyang Zhu, School of Power and Mechanical Engineering, Wuhan University, Wuhan, China

Hao Wang, Guangdong Provincial Key Laboratory of Micro/Nano Optomechatronics Engineering, College of Mechatronics and Control Engineering, Shenzhen University, Shenzhen, China

Linggang Wu, Institute of Applied Physics, Jiangxi Academy of Sciences, Nanchang, China

Mo Li, School of Materials Science and Engineering, Georgia Institute of Technology, Atlanta, USA; mo.li@gatech.edu

\*Corresponding author

doi:10.1557/s43577-023-00566-9



and superior properties are discovered, undoubtedly there will be an increasing interest in looking into the atomic structure in the near-surface regions in order to explain and predict the properties and performance of these materials.

MG is usually obtained from cooling the corresponding glass forming liquid. At the glass-transition temperature  $T_g$ , the liquids become topologically disordered or amorphous solid with no long-range atomic structural order.<sup>11</sup> For this reason, it is not expected that the surface of the MGs would be dramatically different from the bulk. In contrast, surface reconstruction, roughening, and structure or phase transformations are commonly seen in crystals with long-range order.<sup>12,13</sup> Nevertheless, some structural ordering was observed in the surfaces of another topologically disordered material, liquid metals. The atoms on and near the surface are found to organize themselves to form layers with density modulation.<sup>14–16</sup> The cause was thought to be related to the change of the interatomic interactions for the atoms near the surface due to the screening effect from the Friedel oscillation of the electron densities and the high mobility of these atoms in the liquid state that allows for the fast dynamics in reorganizing surface structures. MG, on the other hand, is metastable and its mobility is nearly zero as a solid, or a frozen liquid. Therefore, one should not expect to see structural ordering on or near the surface as in the liquid metals, unless the ordering has been developed in the liquid state and subsequently preserved at temperatures below  $T_g$  by rapid cooling. Indeed, we did not observe any ordering formation in either the surface or subsurface regions of both the MG liquids or the bulk glass. However, we did observe the layered structure in MG nanoparticles. We reported this finding briefly.<sup>17</sup> Here, we explore how this rare and unusual structure change occurs and the causes for it.

By far, most experiments conducted to investigate the surface-related properties of MGs are on surface roughness,<sup>18</sup> phase separation,<sup>19,20</sup> surface-induced crystallization,<sup>21</sup> and surface dynamics.<sup>9</sup> Little is known about the detailed local atomic packing change on and near the surface, in particular, in nanoparticles. Molecular dynamics (MD) simulations provide some specific atomic-level information of surfaces and surface-related properties for MG nanowires. For example, the surface of the MG is observed to remain amorphous but with highly segregated alloy components.<sup>22–24</sup> The driving force for the chemical segregation is identified as the curvature of the nanowires.<sup>25,26</sup> Clearly, further investigation is needed for whether the same or other interesting properties and mechanisms, including the layer formation, could manifest in MG nanoparticles.

In this article, we report some new findings on not only the chemical ordering but, more interestingly, the atomic structure ordering on and near the surface of  $\text{Cu}_{64}\text{Zr}_{36}$  MG nanoparticles. To reveal the details of the surface atomic structure arrangement, we used MD simulation. We found that the formation of multilayers, an onion-like layered atomic structure (LAS), is originated from the surface of the MG nanoparticles in the solid state. This obvious one-dimensional structure is strongly related to temperature. The extent of the periodic

ordering is sensitively dependent on the particle size. When the temperature increases to and above  $T_g$ , the LAS experiences an abrupt change and the layer periodicity starts to disappear. We attribute the structure ordering to the surface stress, rather than interatomic interaction change caused by the electron screening effect in Friedel oscillation. Our further calculation gains insights into the relationship between the surface stress and surface energy gradient and the structure ordering. These findings provide new knowledge for the nature of MG in the nanoscale and the possibilities for manipulating their structures in fabrication of the MG nanostructures.

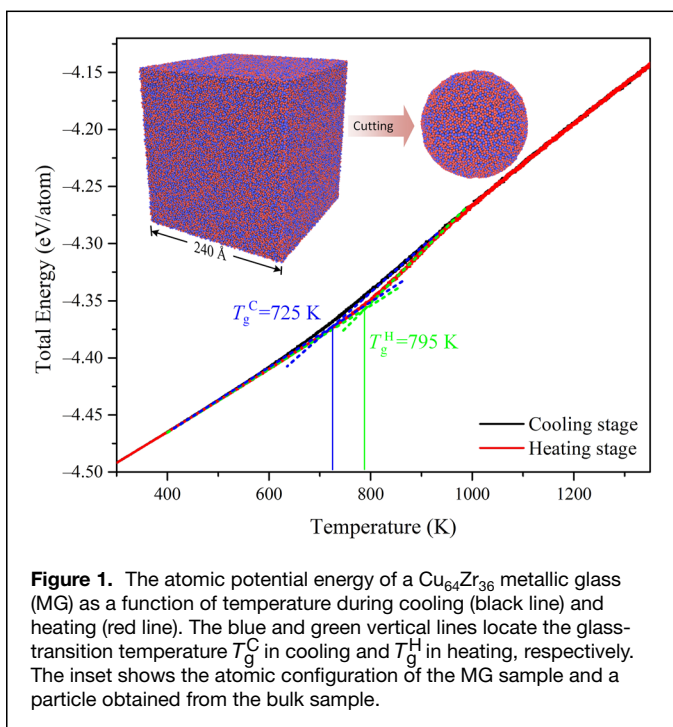
This article is organized as the following. In the next section, we outline the methods used in the MD simulation and calculations of atomic structures and physical properties. In the “[Results and discussion](#)” section, we give the details of the results, in particular, of the formation and characterization of the LAS of the MG nanoparticles, the effects of temperature and particle size on the LAS, and the surface stress and its influence on the structure change. In the “[Conclusion](#)” section, we discuss the mechanisms and factors that influence the LAS formation.

### Sample preparation and simulation methods

In this work, we select a  $\text{Cu}_{64}\text{Zr}_{36}$  alloy to investigate the atomic structure change of the surface and subsurface regions in nanoparticles because this particularly simple binary MG alloy exhibits good glass formability and has been extensively studied both experimentally and theoretically.<sup>27–29</sup> The large-scale atomic/molecular massively parallel simulator (LAMMPS)<sup>30</sup> is used to model the atomic structure change and the physical properties. The interactions between the atoms are described by the embedded atom method poten-

tial,<sup>31,32</sup>  $E_i = F_\alpha \left( \sum_{j \neq i} \rho_\beta(r_{ij}) \right) + \frac{1}{2} \sum_{j \neq i} \phi_{\alpha\beta}(r_{ij})$ , where  $F$  is the embedding energy,  $\phi$  is a pair potential, and  $\alpha$  and  $\beta$  are the element type of atoms  $i$  and  $j$ . The atomic configurations are visualized with OVITO.<sup>33</sup> The constant pressure and temperature ensemble MD is used with the pressure kept at zero but under either constant or varying temperature controlled by a Nosé–Hoover thermostat.

As shown in the inset of **Figure 1**, the sample of a  $\text{Cu}_{64}\text{Zr}_{36}$  liquid with the size  $240 \text{ \AA} \times 240 \text{ \AA} \times 240 \text{ \AA}$  is set up with the periodic boundary conditions applied in all dimensions. The liquid is kept at 2100 K for an extended period of time for equilibration and then quenched to 300 K at a rate of 2 K/ps to obtain glass. The time step is set as 1 fs. **Figure 1** also shows the atomic potential energy of the  $\text{Cu}_{64}\text{Zr}_{36}$  MG as a function of temperature. We use the intersection of two tangent lines of the potential energies at high and low temperatures to locate  $T_g$ , which is at about 725 K during cooling.  $T_g$  changes to about 795 K when we heat up the glass sample from 300 to 2100 K with the heating rate at 2 K/ps. The MG sample is then cut into spheres from the bulk at 300 K with various radii ranging from 15 to 120  $\text{\AA}$ . The spheres with free surfaces, no longer under the periodic boundary conditions, are then heated to different



temperatures ranging from 400 to 1800 K with a rate of 2 K/ps. At each selected temperature, we keep the particles for 2 ns to ensure that they reach a steady state; and in another 2 ns following the equilibration, the atomic positions, velocities, and stresses are calculated and recorded. We also obtain the MG spheres directly from the liquid by quenching. These MG spheres are under similar conditions in experimental synthesis of MG particles, such as in gas atomization. The nanoparticles from the two methods give qualitatively the same results.

## Results and discussion

### Formation of multilayers and surface state of MG particles

#### Identifying LAS with mass-density profiles

To detect any atomic structure ordering in the nanoparticles, we first use the mass-density profile (MDP),  $\rho(r)$ . The MDP is obtained by calculating the mass density of the atoms in the spherical shell between  $r$  and  $r + \Delta r$  at the radial distance  $r$  from the mass center of a sphere. The thickness of each shell  $\Delta r$  is set as 0.2 Å as shown in the inset of **Figure 2a**. The atomic mass of Cu and Zr is 63.546 u and 91.224 u, respectively. Both the total MDP and partial MDPs contributed from Cu and Zr are calculated. To reduce the effect of thermal vibration, all data are averaged over 20 ps with a 0.5 ps time interval.

Figure 2a–d shows the MDPs for the spheres with different sizes at 700 K after 2 ns relaxation. From the figures, one can clearly see an oscillation for the MDPs in all samples. The period of the oscillation appears to be about 2.17 Å, and the amplitudes can reach as high as about 25% of the average density. The periodicity exhibited in the MDPs suggests that

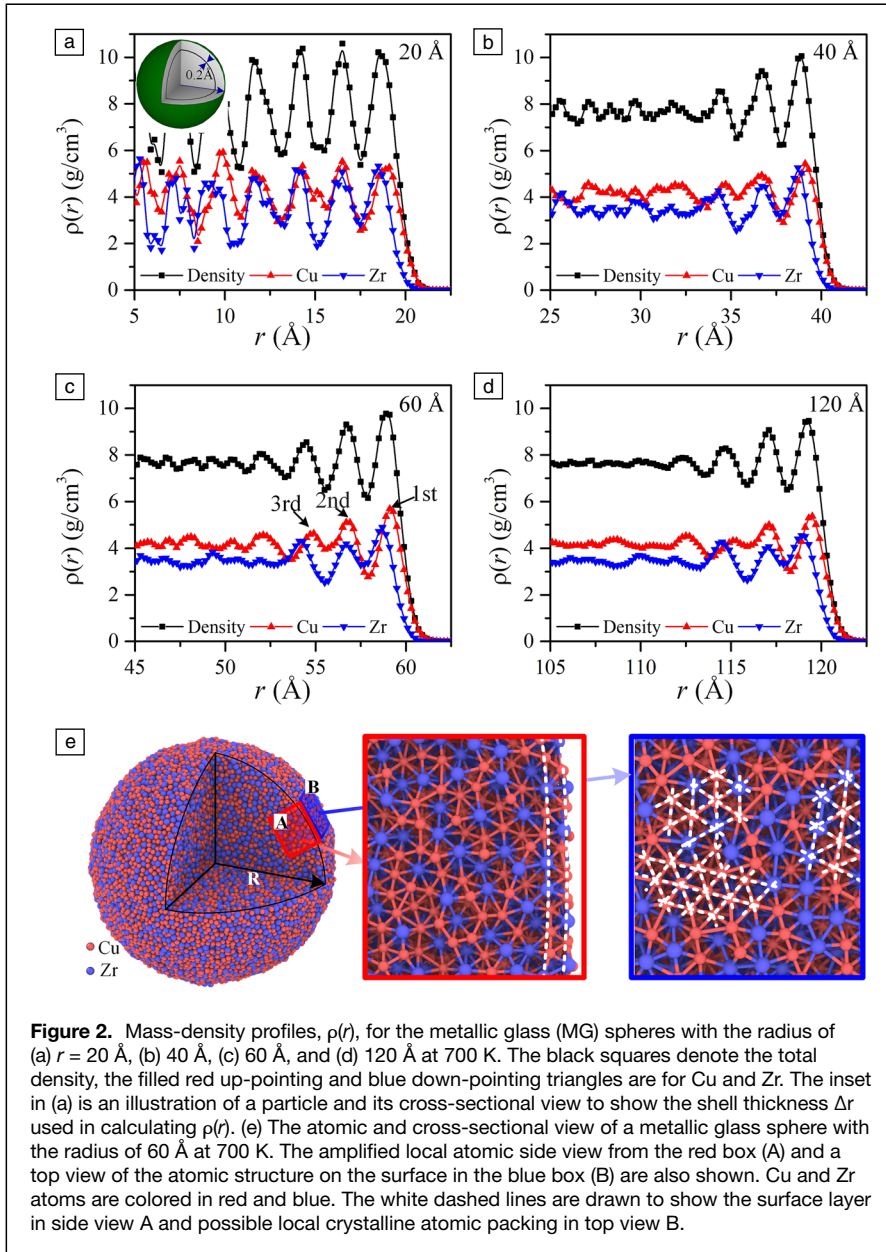
there is a one-dimensional (1D) order formed for the atomic packing along the radial direction of the particles. In the particle with the radius of 20 Å (**Figure 2a**), the MDP shows no damping throughout the whole sample with a fully multilayered, onion-like structure. However, for spheres with larger radii in **Figure 2b–d** the mass-density oscillation damps off from the surface in about three cycles, and the outmost layer around the surface has the highest amplitude.

One possibility for the 1D ordering is partial crystallization within the particles on the inner surfaces as shown by some previous work.<sup>9</sup> Further analysis of the atomic structure in this work, however, shows no existence of 3D or 2D long-range order. **Figure 2e** shows the atomic views of the MG sphere with the radius of 60 Å at 700 K, including the overall view of the particle, the amplified local cross-sectional view, and the top view of the surface. Cu and Zr atoms and their contributions to the MDPs are identified. The dashed lines in the cross-sectional view mark the first and second atomic layers corresponding to the peaks in the MDPs, but the third layer cannot be observed straightforwardly. In the top view of the surface, we notice that about 40% of the atoms are arranged at the vertices of a triangular tiling marked with the white dashed lines. The local ordered atomic arrangement is similar to the atomic packing of the (111) planes in FCC crystal or the (0001) plane in HCP crystal. The pattern of the local hexagonal packing shows unambiguously some sort of short-range order but without long-range translational symmetry. This local order on the first layer, or the surface, only indicates that the LAS at the first layer is dominated by the closest-packed structure mosaics, possibly some local two-dimensional crystalline packing; but the ordering does not extend to the interior of the particles along the radial direction. In other words, the LAS observed along the radial direction is not caused by the local crystallization and must have its origins elsewhere. We shall examine the causes next.

#### Chemical segregation

With the observation of the structural ordering in the MG nanoparticles, our next question is whether there are other changes, such as chemical ordering. It is common that the chemical species segregate in/to the surface in the nanostructure as the surface area becomes significantly bigger and energetically more favorable. Both experiments<sup>34,35</sup> and simulations<sup>22,23,36</sup> have reported chemical segregation in nanowires and nanoparticles where certain chemical elements are enriched in the surface region as compared to the interior or the bulk. There are usually two driving forces for this, albeit mostly for crystalline materials: (1) The segregating element lowers surface energy; and (2) when the surface energy remains the same, the element with a larger size goes to the surface to lower the overall strain energy.<sup>37</sup> In  $\text{Cu}_{64}\text{Zr}_{36}$  MG wires, nevertheless, it was found that the lighter and smaller Cu atoms become concentrated at the surface.<sup>22</sup> We expect the same to occur in the MG nanoparticles.





The first hint of the chemical ordering can be seen in Figure 2 by comparing the total MDP with the partial ones for Cu and Zr. One can see the oscillation of the total and partial MDP and the higher and lower amplitude in partial MDPs for Cu and Zr near the surface, meaning that Cu becomes enriched in the surface and Zr depleted in the same manner, but they are not strictly synchronized with each other. For the convenience of view, we mark out the first, second, and third layer of the surface in Figure 2c at the locations at  $r = 58.9 \text{ \AA}$ ,  $56.7 \text{ \AA}$ , and  $54.5 \text{ \AA}$ , respectively. In the first layer (the outmost layer), the peaks of the partial MDPs of Cu and Zr deviate from the mean peak positions of the total MDP. The Cu peak inclines slightly toward the surface or to the right, and Zr peak to the left or toward the center of the particle. In the second layer,

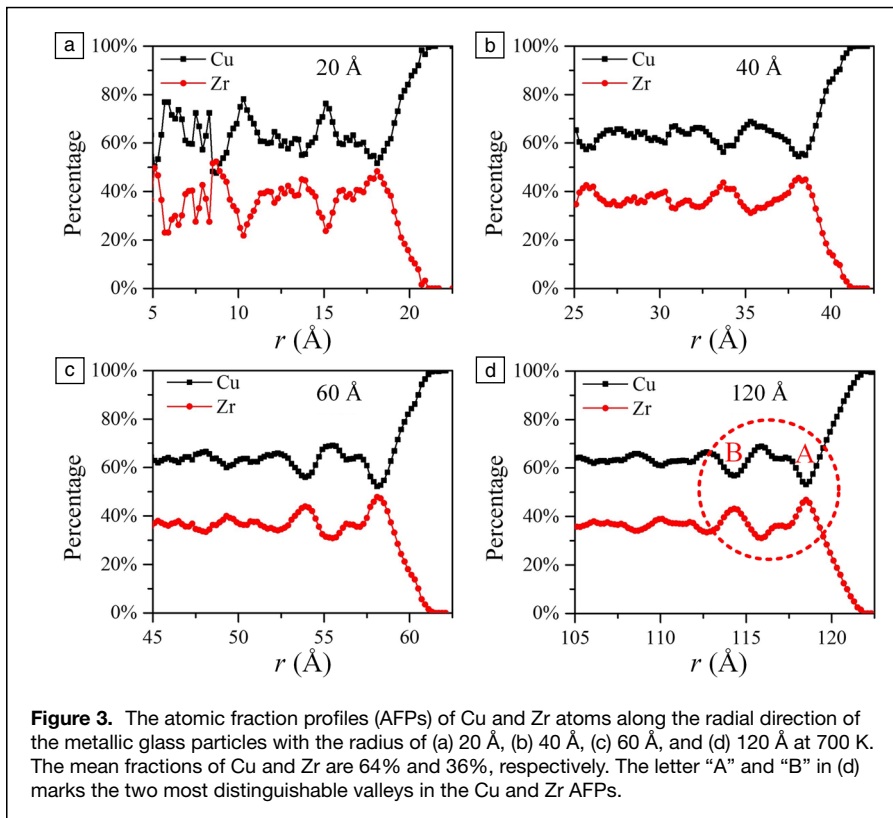
the Cu and Zr peak positions coincide with the peaks in the total MDP. In the third layer, the Cu and Zr peaks deviate from the total MDP again with the same trend as seen in the first layer. The difference in the mismatch of the MDPs is mainly caused by the difference in the atomic sizes and mobility of Cu and Zr atoms,<sup>38</sup> which makes it easier kinetically for Cu segregation to the surface or the top layer.

Figure 3 shows the atomic fraction profiles (AFPs) of Cu and Zr atoms along the radial direction for different size particles,  $N_{\text{Cu}}(r)/N(r)$  and  $N_{\text{Zr}}(r)/N(r)$ , where  $N_{\text{Cu}}(r)$  and  $N_{\text{Zr}}(r)$  are the numbers of Cu and Zr atoms, and  $N(r)$  is the total number of atoms in a shell between  $r$  and  $r + \Delta r$  at the radial distance  $r$ . The black squares and red circles show the fraction of Cu ( $N_{\text{Cu}}(r)/N(r)$ ) and Zr ( $N_{\text{Zr}}(r)/N(r)$ ) atoms, respectively. The AFPs give the local atomic percentage of different atoms from which we can see any chemical concentration change along the radial direction as compared to the mean sample concentration for Cu at 0.64 and Zr at 0.36. If the local atomic concentration in the AFP is larger than the mean value, it is enriched; otherwise depleted.

From Figure 3a–d, we can see the chemical segregation in the surface region: The lighter and smaller Cu atoms are indeed more likely to concentrate at the surface of the particles, forming a Cu-rich surface. In contrast, Zr becomes depleted in the surface region. Nevertheless, both the Cu-rich and Zr-poor region are limited only in the outmost part of the surfaces with a thickness of about  $2 \text{ \AA}$ .

In the subsurface regions below, we still see the concentration modulation but with a nearly negligibly smaller magnitude change.

The AFPs of all samples with different particle radius show a similar characteristic pattern as shown in the MDPs, except there is a larger data fluctuation at the smaller distance  $r$  because the number of atoms in the shell decreases as the distance  $r$  becomes smaller toward the center of the particles, which contributes to poor statistic counting. The oscillation of the AFPs is relatively less clearly distinguishable than those in the MDPs, except for the first few peaks close to the surface. The fraction of Cu atoms drops (marked with an “A” on Figure 3d) first with a value about 0.55 in the first valley next to



the surface peak, then goes up again with two smaller peaks, and falls again to another valley (marked with a “B” on Figure 2d). The closer toward the center of the particles, or further away from the surfaces, the closer AFPs are getting to the mean alloy concentrations. Note that the concentration modulation resembles that in a spinodal decomposition with spontaneity.

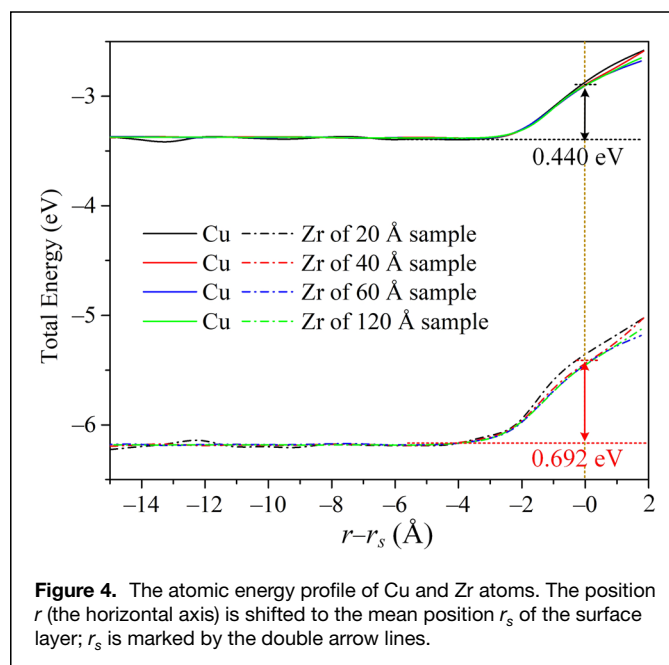
As a defect, the surface with broken atomic bonds raises the energy of the system. As mentioned previously, in alloys or solutions, a certain type of elements would move from the interior to the surface in order to minimize the overall free energy of the system. For MGs made of multicomponent, the tendency of which element would segregate from the interior to the surface is governed by the difference between the energies with the elements in the surface and the interior. For our binary CuZr metallic glass, we compare the changes of the energies of Cu and Zr in the surface and in the bulk. If the surface with more Cu has lower energy than that of Zr, Cu would be the preferred element to segregate to the surface. To confirm this prediction, we calculate the energy of each element in the surface layers and at the center of the particle and compare their difference.<sup>36</sup> Figure 4 shows the potential energy profiles of Cu and Zr atoms in the nanoparticles with various radii. The profiles are calculated using the same techniques as for the MDP and AFP previously. Because the surface is the region with a finite thickness, in presenting the energy profile here, we shift the position  $r$  to  $r - r_s$ , or  $r - r_s$ , where  $r_s$  is the mean position of the surface layer.

From Figure 4, one can see that the potential energies of Cu and Zr increase in the region closer to the surface but Cu

has lower energy than that of Zr. At the mean position of the surface, for example, the energy of Cu is 0.440 eV, whereas that of Zr is 0.692 eV. The much smaller energy contributed from Cu would, therefore, make the overall energy of the surface lower if more Cu atoms are enriched there. Therefore, Cu is the preferred element to segregate to the surface, which is the reason for the peak mismatch of the AFPs found in Figure 3. Besides the thermodynamic reason, there could be a kinetic cause for the segregation of Cu to the surface. Because Cu has a smaller atomic radius, it has relatively higher mobility as compared to that of the larger Zr. Therefore, during the process of chemical segregation, Cu has an advantage of moving to the surface faster.

### Surface stress and surface-induced internal stresses

The formation of the modulated multilayer structure and the surface chemical segregation in the MG nanoparticles indicates that the amorphous solid has both the thermodynamic driving forces and fast dynamics for the atoms to rearrange themselves in the nanoparticles. Different from the liquid metals with the ordered subsurface structure formed near the surface region, the MG nanoparticles form the multilayered LAS that could





extend deep into the center of the particles. The long-range LAS formation must have an origin that is different from the short-range interactions originating from the electron screening effects. Here, we show that the most likely driving force for the LAS formation and the surface chemical segregation is the *surface stress*. The existence of large surface stress in the amorphous solid can have a long-range effect on atomic

where  $\mathbf{r}_{ij}$  is the vector connecting atoms  $i$  and  $j$  and its length is  $r_{ij}$ ,  $k$  is the number of the intersections of  $\mathbf{r}_{ij}$  and the  $R$ -surface,  $\alpha$  is a parameter varying from zero to unity, representing the beginning point to the end point of the contour,  $\mathbf{e}_{l(\alpha_k)}$  is the radial unit vector at the intersection of  $\mathbf{r}_{ij}$  with the  $R$ -surface, given by  $\alpha_k$ , and  $H$  is the Heaviside step function. The tangential component of the stress tensor for a spherical interface is

$$P_{\phi\phi}^c(R) = \frac{1}{2\pi R\Delta} \left\langle \sum_{\text{pairs}} \frac{|\mathbf{r}_{ij} \cdot \mathbf{e}^\phi|}{r_{ij}} f_{ij} H(R + \Delta - l(\alpha_k)) H(l(\alpha_k) - R + \Delta) H(\alpha_k) H(l - \alpha_k) \right\rangle, \quad 4$$

structure rearrangement. In particular, if the surface stress-induced internal stress is modulated that extends from the surface to the interior of the particles, the atoms in the nanoparticles can be driven to achieve the local spherical dense atomic packing, which eventually leads to the LAS with the periodicity along the radial direction. In the following, we present the results from the calculations of the surface stresses and the internal stress distribution in the MG nanoparticles.

The atomic stress consists of the kinetic and configurational contribution,<sup>39–41</sup>

$$P(r) = P^k(r) + P^c(r), \quad 1$$

where the kinetic part is given by  $P^k = kT\rho(r)I$ , where  $I$  is the unit tensor and  $\rho(r)$  is the singlet distribution function of molecular centers. The configurational part can be written as

$$P^c(r) = -\frac{1}{2} \left\langle \sum_{i \neq j} \frac{\partial \mathbf{U}}{\partial \mathbf{r}_{ij}} \int_{C_{ij}} d\mathbf{l} \delta(\mathbf{r} - \mathbf{l}) \right\rangle, \quad 2$$

where  $\mathbf{U}$  is the interatomic potential,  $C_{ij}$  is the integration path from atom  $i$  to atom  $j$ ,  $\mathbf{r}$  is the point in space where the stress is evaluated.  $\delta(\mathbf{r} - \mathbf{l})$  is the Dirac delta function.  $P^c(r)$  highly depends on the particular choice of  $C_{ij}$  especially in an inhomogeneous system such as particles with interface and surface regions, which leads to two different stress forms, the Irving and Kirkwood (IK) stress tensor and Harasima (H) stress tensor. The IK tensor<sup>41</sup> presents the contour as a straight line (IK-contour). The H tensor splits the contribution to a flat and a perpendicular line (H-contour).<sup>42</sup> Note that the choice of stress form (i.e., IK or H) is equivalent in the large scale as the atomic potential is a conservative field, where the integration path will not affect the overall result. Here, we use IK stress tensor to investigate the surface stress of MG spheres, as there is sufficient evidence showing that IK-contour is more suitable for inhomogeneous materials.<sup>40,43–46</sup> In a spherical coordinate, the normal component of the stress tensor for a spherical interface ( $R$ -surface) as a function of the radial coordinate  $R$  can be written as<sup>47,48</sup>

$$P_{rr}^c(R) = \frac{1}{4\pi R^2} \left\langle \sum_{\text{pairs}} \sum_{k=1}^2 \frac{|\mathbf{r}_{ij} \cdot \mathbf{e}_{l(\alpha_k)}|}{r_{ij}} f_{ij} H(\alpha_k) H(l - \alpha_k) \right\rangle, \quad 3$$

where  $\Delta$  is equal to half the bin width,  $\mathbf{e}$  is the unit vector in the  $\phi$  direction, and  $l(\alpha_k)$  is the length of the radial vector describing the intersection of  $\mathbf{r}_{ij}$  with the  $\phi$  surface.

Using the previously discussed expressions (Equations 1–4), we calculated the profiles of the stress component  $\sigma_{rr}(r)$  and  $\sigma_{\phi\phi}(r)$ , while  $\sigma_{r\phi}(r)$  component remains zero, for the MG particles with a radius of (a) 20 Å, (b) 40 Å, (c) 60 Å, and (d) 120 Å at 700 K along the radial direction. Same as in calculating the MDP and AFP, here, we chose the bin size  $\Delta r = 0.1$  Å, and calculate these stresses in the spherical shell between  $r$  and  $r + \Delta r$ . The data are averaged over 20 ps with a 0.5 ps interval to reduce the effects of thermal motion.

**Figure 5** shows that the normal stress  $\sigma_{rr}(r)$  is zero in the surface region and gradually becomes negative toward the center (the negative sign denotes compressive hydrostatic pressure, while the positive for tensile pressure). The magnitude of the normal stress at the center ( $r=0$ ) is about 1.16, 0.55, 0.36, and 0.20 GPa for the particles with the radius of 20 Å, 40 Å, 60 Å, and 120 Å, respectively. This is the manifestation of the familiar Young–Laplace relation, that is, the smaller the particle radius, the larger the internal (compressive) pressure. Except for the particle with the radius of 20 Å,  $\sigma_{rr}(r)$  changes smoothly with barely observable variations or oscillations from the surface to the center of the particle. In other words, the oscillation in  $\sigma_{rr}(r)$  becomes more apparent when the size of the particles is getting smaller.

In contrast to the normal stress, the tangential stress  $\sigma_{\phi\phi}(r)$  shows clear oscillations. From the surface toward the center of the particle, the amplitude of  $\sigma_{\phi\phi}(r)$  decreases gradually with the largest peak of 7 GPa at the position corresponding to the mean surface region and a valley of –2 GPa right below the surface layer. Clearly, the top surface layer with the largest positive peak is under tension, and the layer immediately below it is under compression. The tension–compression cycle repeats inside the particles as  $r$  gets smaller. Further inside the particle, the normal and tangential stresses approach some smaller values. Note that the largest tangential tension stress in the surface layer remains at 7 GPa and the compression stress in the subsurface layer at –2 GPa, despite the differences in the particle size. However, the oscillation of the tangential stress depends on the particle size: The smaller the particle size, the more intense the oscillation. As the particle radius

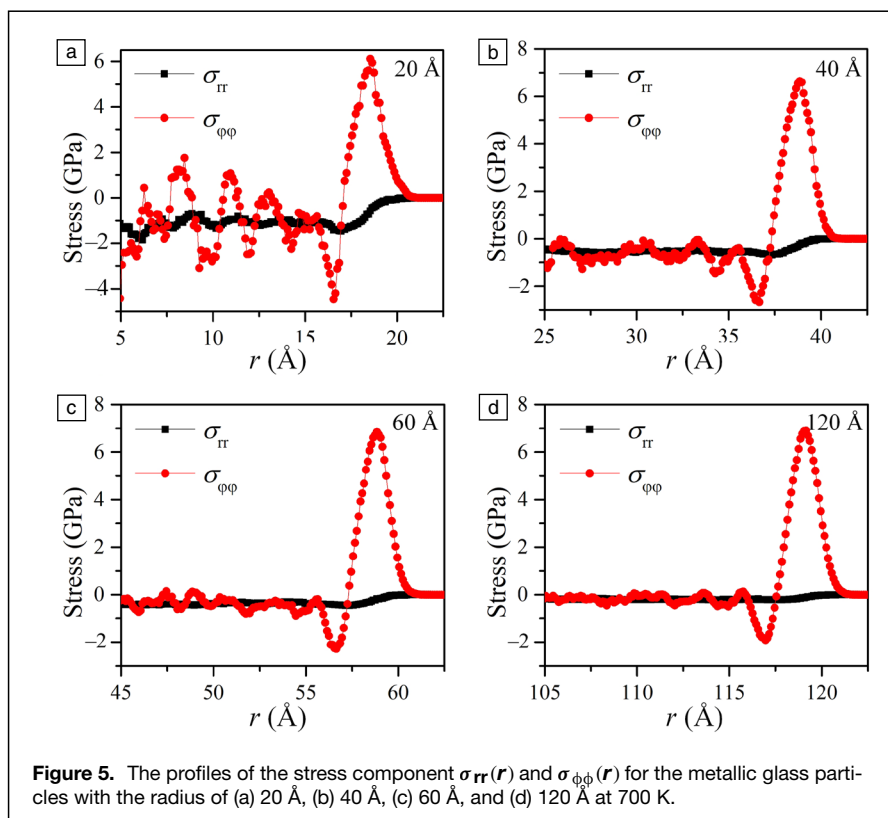


**Figure 5.** The profiles of the stress component  $\sigma_{rr}(r)$  and  $\sigma_{\phi\phi}(r)$  for the metallic glass particles with the radius of (a) 20 Å, (b) 40 Å, (c) 60 Å, and (d) 120 Å at 700 K.

approaches 120 Å, the tangential stress oscillation damps to a smooth curve below about 100 Å (Figure 5a–d).

Finally, but more importantly, by comparing the profiles of the tangential stress (Figure 5) and the mass density (Figure 2), one can see unambiguously that the LAS shown in the MDPs has the perfect match in the periodicity of the oscillations for the first two peaks close to the surface. For example, the position of the distinctive 7 GPa stress peak coincides exactly with that of the first layer in the MDP and the –2 GP stress valley overlaps with the peak position of the second layer. There are slight shifts, about 2–2.5 Å, for the peak positions between the two profiles when the distance inside the particles are closer to the center. In the following, we shall connect the two in relation to the formation of the LAS.

### Surface stress-induced LAS

The results previously presented demonstrate that rather than the chemical segregation, the formation of the LAS in MG nanoparticles could likely be the consequence of surface stress, especially the tangential stress. It exhibits the same oscillatory behavior as that in the LAS. Therefore, we propose a new mechanism for the LAS formation with the surface stress as the driving force.

When a MG nanoparticle forms, the surface energy emerges along with the surface stress as shown in Figures 4 and 5. To reduce the energy and also equilibrate the unbalanced surface stress, atoms tend to rearrange themselves,

starting from the surface. We need to point out that the surface energy and stresses shown in Figures 4 and 5 are those after the atomic configurations have changed, or after the particle is relaxed. Before relaxation, the surface energy and the stresses are bigger. The unbalanced surface stresses before relaxation serve as a driving force for the atoms in the top surface layer to reorganize, preferably, into a denser random packing (Figure 2e) because the stresses are the largest on the surface. The tangential stress plays a more important role here because the atoms on the spherical surface have more degrees of freedom to move on the surface. This can be seen clearly from the dense atomic packing on the top surface layers, some of which even possess the highest two-dimensional hexagonal lattice structure, as shown in the top surface layer in Figure 2e. The surface atomic configuration and the overlap of the peak positions of tangential stress with the density profiles at the first surface layer provide direct support for this conclusion.

While the reorganizing atoms in the top surface layer have an extra degree of freedom in the radial direction perpendicular to the surface, the atoms in the subsurface layers and interior are much more constrained. Once the surface layer forms, further packing of the atoms in the subsurface layers is under the restriction by the curved and also smaller shell regions as the distance  $r$  is approaching the center of the particle. Packing atoms as densely as those on the surface becomes more difficult with the two-dimensional crystal-like mosaics, which leads to a finite extent of the LAS inside the particles. This is an inverse case of the atomic packing around a central atom such as in the structural model for the radial distribution function (RDF) of MG.<sup>5,49,50</sup>

Another reason for having a finite number of LAS in the larger particles is due to the decreasing effects of the surface stress that is inversely proportional to the particle radius, or directly connected to the curvature of the particle. The smaller surface stress effect in the larger particles reduces the driving force for the rearrangement of the atoms farther away from the surface. It is worth mentioning that the fully ordered layer structure is also reported in some core–shell nanostructures,<sup>51</sup> where the spherical periodic orders arise from both the center and the surface and merge at the middle, which results from the ordered carbon nanotube around it. The interface acts as the controller for the formation of the layered structure. The unique feature in our case is that the outer confinement shell is the free surface only with the presence of surface stress.





### Influence of particle size and temperature on LAS

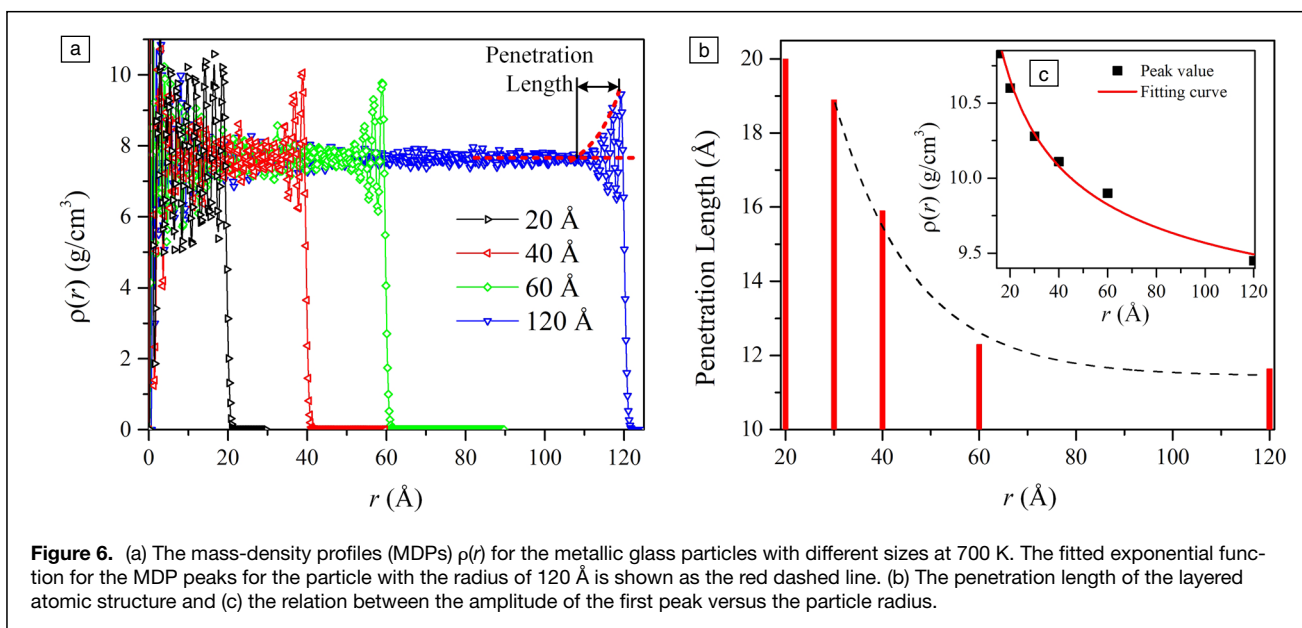
The formation of the LAS in MG nanoparticles demonstrated in the previous section is at 700 K. We show that the surface stress is the major driving force for LAS formation. In the last section, we mentioned that the particle size can change the surface stress via the Laplace type of relation, and as a result, the LAS becomes damped as the internal stress becomes smaller in larger particles (Figure 2). Temperature rise, on the other hand, causes the structure relaxation, which is particularly sensitive for the metastable solid such as MG. The structural relaxation can lead directly to reduction of the surface as well as internal stress that in turn can cause the change in the LAS. In particular, when temperature reaches  $T_g$ , MG undergoes a solid-to-liquid transition where the mechanical stability vanishes, along with the internal stress, which causes the disappearance of the LAS. In this section, we shall give more details of how the particle size and temperature influence the LAS.

### Size effect on the LAS

Size effect found in nanomaterials is often associated with the large ratio between the surface area versus the volume that is thought to be responsible for the surface-related property changes. In MG nanoparticles, we found that in addition, the particle size also contributes to atomic structural change (i.e., the formation of the LAS) caused by the surface stress. In the “Formation of multilayers and surface state of MG particles” section, we show that a fully layered structure is developed in the particle with the radius of 20 Å or smaller; and only partially layered structure forms when the particle radius is bigger. In the latter, the layers only extend to a finite distance into the interior from the surface. We argued that the cause is related to the Young–Laplace (YL) type of relation between the surface stress and internal stress, and the particle size. The relation can be perceived clearly in Figure 5 where the mean

compressive pressure is about 1 GPa inside the sphere with a radius of 20 Å, but only 350 MPa for the particle with a radius of 60 Å. Therefore, the smaller the particle size is, the larger the internal stress caused by surface stress, and the deeper the LAS would extend into the inside of the particle from the surface. The LAS type of structure seen in the nanoparticles is different from the reported cases of pressure effects on atomic structure of bulk MGs.<sup>52</sup> In our case, the LAS is driven by tangential stress.

The YL relation relates only the mean sample hydrostatic pressure to the particle radius via the surface stress. In our case, from the tangential as well as the hydrostatic stress profiles we can see more detailed local stress variation versus the radius inside the particle (Figure 5) and its impact on the development of the LAS. In Figure 6a, we plot the mass-density profiles in a single frame for all particles with different sizes so we can directly compare the extent of the LAS in these particles. The LAS is characterized by the clearly definable MDP peaks and valleys, or the oscillations. The oscillation vanishes and the amplitude decays to a constant value in the distance of about 10 Å from the surface for the particle with the radius of 120 Å, whereas the oscillation extends to the entire sample for the particle with the radius of 20 Å. As illustrated in Figure 6a (see the red dashed line for the MDP for the particle with the radius of 120 Å), by fitting an exponential function to the MDP peak heights from the surface layer to the interior of the particle, we can roughly obtain the penetration length of the oscillations, or the mean extent of the LAS. In Figure 6b, we plot the penetration lengths of different size particles versus the particle radius. One can see that the size effect, or the extent of the LAS in the MG particles, start to show up at 60 Å; and below 20 Å the particles are able to develop full length LAS, that is, the LAS penetration length equals to that of the particle radius. To better understand the YL relation in the nanoparticles that we mentioned previously,





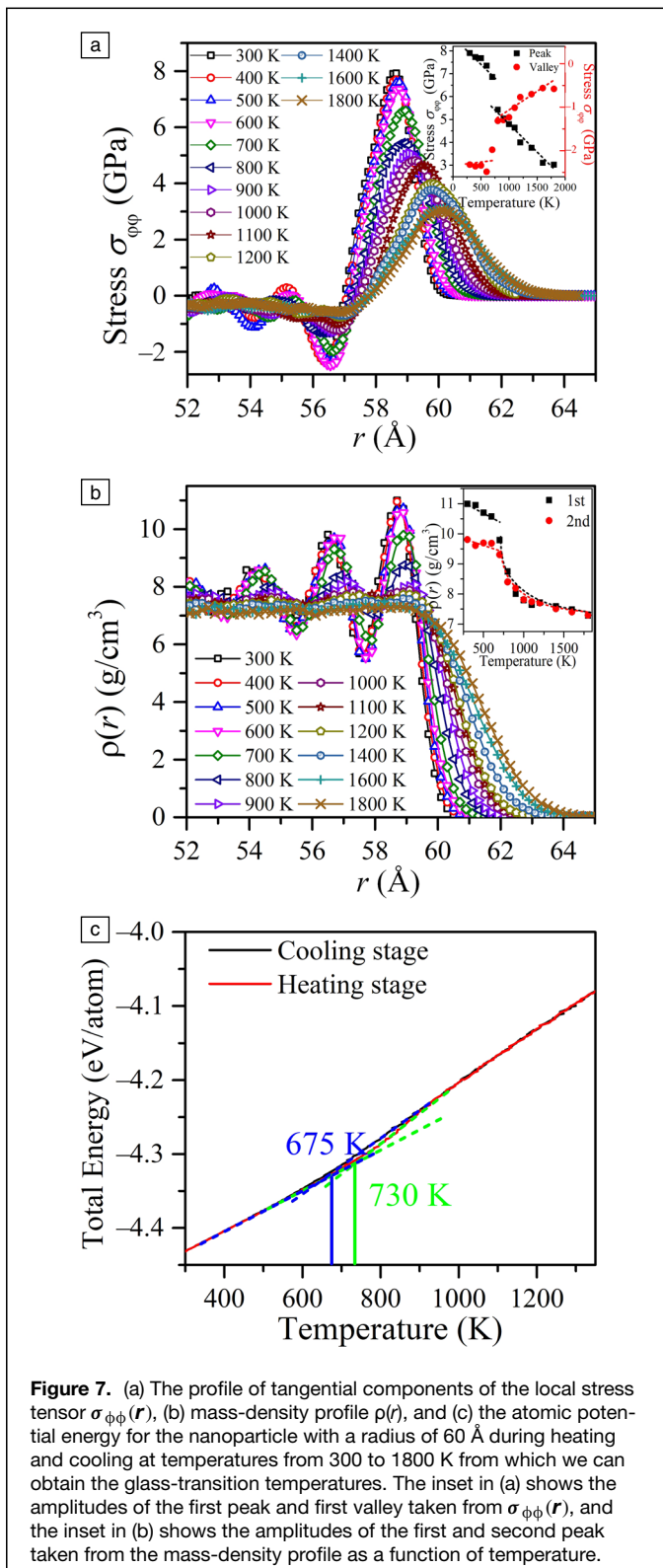


**Figure 7.** (a) The profile of tangential components of the local stress tensor  $\sigma_{\phi\phi}(r)$ , (b) mass-density profile  $\rho(r)$ , and (c) the atomic potential energy for the nanoparticle with a radius of 60 Å during heating and cooling at temperatures from 300 to 1800 K from which we can obtain the glass-transition temperatures. The inset in (a) shows the amplitudes of the first peak and first valley taken from  $\sigma_{\phi\phi}(r)$ , and the inset in (b) shows the amplitudes of the first and second peak taken from the mass-density profile as a function of temperature.

in Figure 6c, we also plot the amplitude of the first peak in the MDPs versus the particle radius in Figure 6a. Clearly, the amplitude of the first peak of the MDP, or intensity of the surface stress, show a strong size dependence.

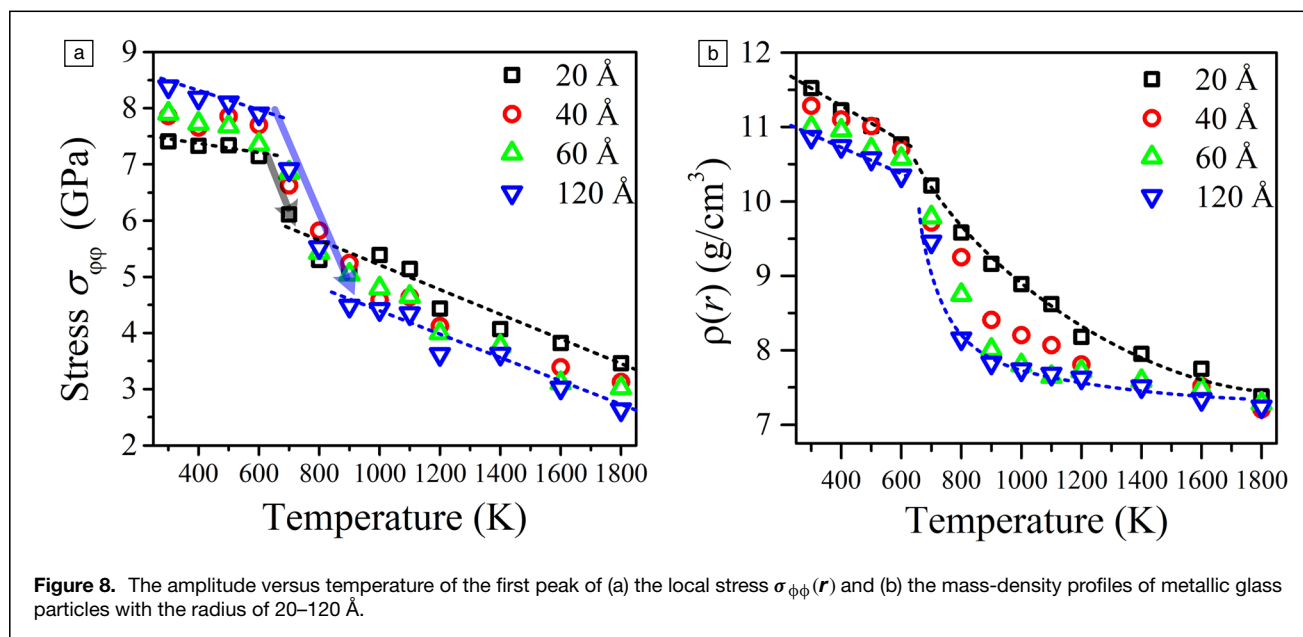
### Temperature effects

Figure 7a shows the profile of the tangential stress component  $\sigma_{\phi\phi}(r)$  of the particle with a radius of 60 Å at different temperatures ranging from 300 to 1800 K. For a better view, we only plot the part of  $\sigma_{\phi\phi}(r)$  from  $r = 52$  to 65 Å. One can see clearly that as the temperature increases, the peaks and valleys of the oscillatory  $\sigma_{\phi\phi}(r)$  become flattened out gradually at smaller  $r$  values away from the surface. In the inset in Figure 7a, we show the change of the amplitude of the first peak and the first valley of  $\sigma_{\phi\phi}(r)$  in the surface and subsurface region as a function of temperature. There is a discontinuous region starting above 700 K where the amplitudes of the peak and valley drop precipitously. Note that the surface stress does not vanish completely at high temperatures. Both the hydrostatic and tangential stress reaches a constant negative value, or the mean stress inside the particles. For the hydrostatic pressure and the tangential stress, the negative value means compression. The smaller amplitudes and the flattened oscillation as  $r$  gets smaller is the manifestation of the YL relation.

Figure 7b shows the MDP  $\rho(r)$  in the corresponding temperature range as shown in Figure 7a. Same as for  $\sigma_{\phi\phi}(r)$ , the amplitudes of the MDPs also become smaller with increasing temperature but the oscillation is still observable when the temperature is above 1000 K, albeit with much smaller amplitude. We also plot the amplitudes of the first two peaks of the MDPs versus temperature in the inset of Figure 7b. Above 700 K, they start to show a large decrease as seen in the inset of Figure 7a, and more interestingly, the two curves overlap with each other at high temperature. Above 1200 K, the oscillation in MDPs vanishes and the density approaches a mean value at 7.21 g/cm<sup>3</sup>. Note that at higher temperatures, all peaks and valleys in both the stress and mass-density profiles are shifted slightly to the larger  $r$  values due to thermal expansion of the particles but the periodicity or wavelength remains almost invariable when the amplitude decays.

The discontinuous drop of the amplitudes in the stress and the MDPs at high temperatures is related to the glass transition in the nanoparticles. The glass-transition temperature  $T_g$ , however, conventionally refers to the transition temperature from cooling a liquid. As shown in Figure 7c, the glass-transition temperature obtained from cooling the liquid particle is located at 675 K, and when the particle is heated it is 730 K. It is more appropriate to use the latter in our analysis because we heat the particles up. Note that the  $T_g$ 's obtained for the bulk (Figure 1) and the particle differs only slightly. As seen in Figure 7a–b, indeed when  $T_g$  is approached, the particle starts to transform from solid to liquid. The internal stress in the MG is quickly relaxed as the atoms start to move around, which causes the disappearance of the LAS. It is worth noting that in the liquid state, except the surface stress the internal stress in the particle no longer shows oscillation but still remains at a finite value at high temperature above  $T_g$  (Figure 7a) due to the YL relation.

The same trend presented above in the particle with the radius of 60 Å can be found in other particles of different



**Figure 8.** The amplitude versus temperature of the first peak of (a) the local stress  $\sigma_{\phi\phi}(r)$  and (b) the mass-density profiles of metallic glass particles with the radius of 20–120 Å.

sizes. In **Figure 8a–b** we show the amplitudes of the first peak of  $\sigma_{\phi\phi}(r)$  and the MDPs for the outmost layer of the particles with the radius of 20–120 Å at the temperature of 300–1800 K. When the temperature is below  $T_g$ , the amplitudes decrease slightly with a linear relationship with temperature. As shown in the insets in **Figure 7**, at  $T_g$  an abrupt and faster decrease occurs. When temperature is above  $T_g$ , the linear relation resumes but with a different slope. The particle size effect can also be seen clearly in the plot (**Figure 8**): the decreasing trend of both the amplitudes for the tangential stress and the mass-density profiles is slower for smaller particles; and above 60 Å, the trends become the same.

The effect of temperature shown above provides another support for our proposed causal relation between the formation mechanism of the LAS and the surface stress: Not only does the appearance of the modulation of the internal stress go in tandem with that of the density modulation inside the particles but also their disappearance.

## Conclusion

Atomic structure of MG spheres is investigated via MD simulation with an emphasis on the surface and surface-induced structure changes inside the particles. We found that MG spheres become multilayered in terms of the mass density below the glass-transition temperature with a perfect periodicity along the radial direction. The formation of the onion-like structure is also accompanied by surface segregation. The degree of surface layering changes with temperature and sample size. The periodicity becomes less obvious at higher temperatures and vanishes above  $T_g$ , and its extent becomes shorter with the increasing particle size.

Our work indicates that the formation of the multilayer atomic structure in the MG nanoparticles is caused by the surface stress. The existence of the surface stress leads to the

development of the internal stress, which drives the atoms to rearrange to minimize the internal stress and energy. For a spherical particle, the lower energy configuration formed is the top surface layer with local dense packing, including some crystalline lattice packing. Once the dense surface packing is established, the subsequent atomic packing in the subsurface and interior regions is under more strict geometric constraints. Therefore, the subsequent inward layer-by-layer packing from the surface becomes strongly dependent of the particle size. In addition, the particle size imparts another constraint to the layer formation by the change of the internal stresses through the YL relation. Below 20 Å, the full length LAS is observed throughout the entire particle, whereas the layering only occurs with finite penetration length for larger particles. Temperature affects the LAS formation through relaxation of atomic structures by thermal motion. The higher the temperature, the less sharp the LAS features and the layers vanish above the glass-transition temperature where the MG becomes liquid.

MG has been thought to be homogeneous and isotropic. As compared to the crystals with the structural ordering that persists down to nanoscales, the amorphous material should have no long-range structural order in both the bulk and smaller sizes, including surfaces. Our work provides a different view of structural ordering in this class of structureless materials. We show that at least one-dimensional atomic order can be developed in nanospheres driven by the surface stress. Similarly, this multilayer structure is expected to exist in nanowires for the same reason as for the spheres. This kind of ordering, however, is fundamentally different from that in crystallization where each atom registries precisely with the lattice positions and extends to long-range. The ordering in MG nanoscale objects is governed largely by the external field such as stress and the kinetic conditions for atoms to



move. It is the metastability of the amorphous state that makes it possible to develop ordering in MG with the influence of these conditions: The shallow metastable state characteristic to amorphous materials enables the atomic configurations to change relatively easily that forms the LAS. In contrast, it is difficult to change the crystalline structure from one deep stable state to another. Nevertheless, the demonstration in this work of the existence of ordering in amorphous solids such as the MG gives us hope to develop certain atomic ordering in this class of materials from which certain exotic and superb properties could be obtained.

## Acknowledgments

M.L. would like to acknowledge the financial support from the National Thousands Talents Program of China. Y.Y.Z. would like to thank the support provided by Fundamental Research Funds for the Central Universities (No. 2042021kf0026) and the National Natural Science Foundation of China (No. 51705335). H.W. would like to thank the support provided by the National Natural Science Foundation of China (No. 51771123) and the Shenzhen Peacock Innovation Project (Grant No. KQJSCX20170327151307811).

## Funding

Funding was provided by the National Natural Science Foundation of China (Grant No. 51705335), Fundamental Research Funds for the Central Universities (Grant No. 2042021kf0026).

## Data availability

Data will be made available on reasonable request from the authors.

## Conflict of interest

On behalf of all authors, the corresponding author states that there is no conflict of interest.

## References

- G. Kumar, H.X. Tang, J. Schroers, *Nature* **457**(7231), 868 (2009)
- G. Kumar, A. Desai, J. Schroers, *Adv. Mater.* **23**(4), 461 (2011)
- W.L. Johnson, J. Plummer, *Nat. Mater.* **14**(6), 553 (2015)
- J.D. Bernal, *Nature* **185**(4706), 68 (1960)
- P. Häussler, J. Barzola-Quiquia, *J. Non-Cryst. Solids* **312**, 498 (2002)
- D.B. Miracle, *Acta Mater.* **54**(16), 4317 (2006)
- H.W. Sheng, W.K. Luo, F.M. Alamgir, J.M. Bai, E. Ma, *Nature* **439**(7075), 419 (2006)
- H.-G. Liao, D. Zhrebetsky, H. Xin, C. Czarnik, P. Ercius, H. Elmlund, M. Pan, L.-W. Wang, H. Zheng, *Science* **345**(6199), 916 (2014)
- N. Chen, D. Wang, P.F. Guan, H.Y. Bai, W.H. Wang, Z.J. Zhang, H. Hahn, H. Gleiter, *Appl. Phys. Lett.* **114**(4), 043103 (2019)
- C.R. Cao, K.Q. Huang, J.A. Shi, D.N. Zheng, W.H. Wang, L. Gu, H.Y. Bai, *Nat. Commun.* **10**(1), 1966 (2019)
- X.J. Liu, Y. Xu, X. Hui, Z.P. Lu, F. Li, G.L. Chen, J. Lu, C.T. Liu, *Phys. Rev. Lett.* **105**(15), 155501 (2010)

- A.S. Preston, R.A. Hughes, T.B. Demille, V.M.R. Davila, S. Neretina, *Acta Mater.* **165**, 15 (2019)
- K. Cao, L. Shi, M. Gong, J. Cai, X. Liu, S. Chu, Y. Lang, B. Shan, R. Chen, *Small* **13**(32), 1700648 (2017)
- E. DiMasi, H. Tostmann, B.M. Ocko, P.S. Pershan, M. Deutsch, *Phys. Rev. B* **58**(20), 419 (1998)
- O.M. Magnussen, B.M. Ocko, M.J. Regan, K. Penanen, P.S. Pershan, M. Deutsch, *Phys. Rev. Lett.* **74**(22), 4444 (1995)
- O. Shpyrko, M. Fukuto, P. Pershan, B. Ocko, I. Kuzmenko, T. Gog, M. Deutsch, *Phys. Rev. B* **69**(24), 245423 (2004)
- Y. Zhu, H. Wang, L. Wu, M. Li, *Scr. Mater.* **177**, 132 (2020)
- A.I. Oreshkin, V.N. Mantsevich, S.V. Savinov, S.I. Oreshkin, V.I. Panov, A.R. Yavari, D.B. Miracle, D.V. Louzguine-Luzgin, *Acta Mater.* **61**(14), 5216 (2013)
- M.C. Lee, J.M. Kendall, W.L. Johnson, *Appl. Phys. Lett.* **40**(5), 382 (1982)
- A.A. Kündig, M. Ohnuma, D.H. Ping, T. Ohkubo, K. Hono, *Acta Mater.* **52**(8), 2441 (2004)
- U. Köster, *Mater. Sci. Eng.* **97**, 233 (1988)
- Q. Zhang, Q.-K. Li, M. Li, *J. Chem. Phys.* **141**(19), 194701 (2014)
- O. Adjaoud, K. Albe, *Acta Mater.* **113**, 284 (2016)
- O. Adjaoud, K. Albe, *Acta Mater.* **145**, 322 (2018)
- Y.Z. Li, Y.T. Sun, Z. Lu, M.Z. Li, H.Y. Bai, W.H. Wang, *J. Chem. Phys.* **146**(22), 224502 (2017)
- Y.T. Sun, C.R. Cao, K.Q. Huang, J.A. Shi, L.Z. Zhao, M.Z. Li, H.Y. Bai, L. Gu, D.N. Zheng, W.H. Wang, *Intermetallics* **74**, 31 (2016)
- J. Zemp, M. Celino, B. Schönfeld, J.F. Löffler, *Phys. Rev. B* **90**(14), 10 (2014)
- D. Xu, B. Lohwongwatana, G. Duan, W.L. Johnson, C. Garland, *Acta Mater.* **52**(9), 2621 (2004)
- S. Feng, L. Qi, L. Wang, S. Pan, M. Ma, X. Zhang, G. Li, R. Liu, *Acta Mater.* **95**, 236 (2015)
- S. Plimpton, *J. Comput. Phys.* **117**(1), 1 (1995)
- V. Borovikov, M.I. Mendeleev, A.H. King, *Model. Simul. Mater. Sci. Eng.* **24**(8), 085017 (2016)
- M.S. Daw, M.I. Baskes, *Phys. Rev. B* **29**(12), 6443 (1984)
- A. Stukowski, *Model. Simul. Mater. Sci. Eng.* **18**(1), 015012 (2009)
- M. Ahmadi, F. Behafarid, C. Cui, P. Strasser, B.R. Cuenya, *ACS Nano* **7**(10), 9195 (2013)
- D. Lahiri, B. Bunker, B. Mishra, Z. Zhang, D. Meisel, C.M. Doudna, M.F. Bertino, F.D. Blum, A.T. Tokuyoshi, S. Chattopadhyay, T. Shibata, J. Terry, *J. Appl. Phys.* **97**(9), 094304 (2005)
- G. Wang, M.A. Van Hove, P.N. Ross, M. Baskes, *J. Chem. Phys.* **122**(2), 024706 (2005)
- M. Cui, H. Lu, H. Jiang, X. Meng, *ACS Nano* **10**(12), 10618 (2016)
- Y. Zhu, G. Liao, T. Shi, Z. Tang, M. Li, *Acta Mater.* **125**, 69 (2017)
- J.P.R.B. Walton, K.E. Gubbins, *Mol. Phys.* **55**(3), 679 (1985)
- P. Schofield, J.R. Henderson, *Proc. R. Soc. London A* **379**(1776), 231 (1982)
- J.H. Irving, J.G. Kirkwood, *J. Chem. Phys.* **18**(6), 817 (1950)
- A. Harasima, *Adv. Chem. Phys.* **1**, 203 (1958)
- E.M. Blokhuis, D. Bedeaux, *J. Chem. Phys.* **97**(5), 3576 (1992)
- T. Ikeshoji, B. Hafskjold, H. Furuholt, *Mol. Simul.* **29**(2), 101 (2003)
- B. Hafskjold, T. Ikeshoji, *Phys. Rev. E* **66**(1), 011203 (2002)
- S.M. Thompson, K.E. Gubbins, J.P.R.B. Walton, R.A.R. Chantry, J.S. Rowlinson, *J. Chem. Phys.* **81**(1), 530 (1984)
- G.J. Tjatjopoulos, J.A. Mann Jr., *Mol. Phys.* **60**(6), 1425 (1986)
- C.K. Addington, *Molecular Simulation of Phase Behavior, Interfacial Phenomena, and Pressure Effects in Porous Media* (North Carolina State University, Raleigh, 2016)
- P. Häussler, *Phys. Rep.* **222**(2), 65 (1992)
- S. Zhang, C. Dong, P. Häussler, *J. Vac. Sci. Technol. A* **40**(2), 022201 (2022)
- M. Hu, K.P. Giapis, J.V. Goicochea, D. Poulikakos, *Appl. Phys. Lett.* **97**(15), 153107 (2010)
- L. Qi, L.F. Dong, S.L. Zhang, X.B. Chen, R.P. Liu, P.K. Liaw, *Phys. Lett. A* **372**(5), 708 (2008) □

## Publisher's note

Springer Nature remains neutral with regard to jurisdictional claims in published maps and institutional affiliations.

Springer Nature or its licensor (e.g. a society or other partner) holds exclusive rights to this article under a publishing agreement with the author(s) or other rightsholder(s); author self-archiving of the accepted manuscript version of this article is solely governed by the terms of such publishing agreement and applicable law.